Scripta METALLURGICA et MATERIALIA
Vol. 29, pp. 1477-1482, 1993
Printed in the U.S.A.
Pergamon Press Ltd.

YIELD OF CONTINUOUS FIBER COMPOSITES UNDER AXISYMMETRIC LOADING

Hongyan Zhang†, Sriram Krishnaswami, Peter M. Anderson, and Glenn S. Daehn
Department of Materials Science and Engineering, The Ohio State University,
116 West 19th Avenue, Columbus, OH 43210-1179
†Currently: Dept. Materials Science and Engineering, University of Michigan, Ann Arbor, MI 48109-2136

(Received August 31, 1993)

Introduction

Fiber composites have yield properties which clearly differ from the typical von Mises behavior used to describe yield of homogeneous plastic materials. Earlier models based on yield of a cylindrical composite element, in which an elastic fiber is surrounded by an annulus of nonhardening elastic-plastic material, predict a bilinear stress-strain behavior during monotonic uniaxial loading along the fiber direction [1], and qualitatively predict experimental measurements of hysteretic behavior during cyclic uniaxial loading [2]. Unlike pure or solid solution materials, two-phase materials are susceptible to yield under pure hydrostatic loading [3, 4]. In particular, TEM studies have documented high dislocation densities around SiO_2 and Al_2O_3 particles in a Cu matrix, when loaded to 2.5 GPa pressure [3]. Corresponding continuum analyses have quantified the deviatoric stresses produced near particles [3] and cylindrical fibers [5] under hydrostatic loading, when the bulk moduli of the two phases are different. Other departures from von Mises behavior are the marked anisotropy of yielding under various multiaxial stress states, as well as yielding due to heating or cooling. For example, finite element studies of a hexagonal array of aligned elastic fibers in an elastic-perfectly plastic matrix, with material properties chosen to simulate a B-Al composite, were used to determine the loading and uniformly distributed temperatures at which yielding first occurs [5, 6]. Although the von Mises yield surface used to describe matrix yield is a circular cylinder extending indefinitely along the hydrostatic axis, the composite yield surface is truncated along the hydrostatic axis, and resembles an irregular ellipsoid when plotted as a function of the direct stresses acting on the composite [6]. The same finite element studies have shown that heating or cooling the composite by an amount ΔT effectively shifts the surface for initial yield along the hydrostatic axis by an amount, $3\Delta T(\alpha_m-\alpha_f)/(1/K_f-1/K_m)$, where α and K are the coefficient of thermal expansion and bulk modulus of the matrix (m) or fiber (f), respectively. More recent work has examined the critical ΔT to yield the composite, as a function of elastic properties and volume fractions of the components [7, 8].

The present work documents the critical axisymmetric stress states to yield continuous fiber composites, as a function of the elastic properties and volume fractions of the components. In the results presented here, the surfaces correspond to yield of the entire matrix. Some other analyses have based surfaces on the initial matrix yield [5, 6]. The yield surfaces produced here are nearly elliptical and can be characterized by three quantities: the lengths of the major and minor axes and the orientation angle of the ellipse. Although yield surfaces of specific fiber composites have been reported previously, this study addresses axisymmetric yield behavior over a wide range of component properties and volume fractions, in an effort to provide useful yield design criteria. Where appropriate, comparison will be made to estimates of yield of fiber composites based on finite element [5, 9, 10] and self-consistent approaches [11], as well as particulate composite models based on upper bound approaches in the limit of rigid spherical particles [12], spherical cavities [13, 14, 15], and elongated cavities [16].

Approach

A more detailed formulation of the axisymmetric analysis is in Zhang *et al.* [8], which considers the stress state and eventual yield in the composite when heated or cooled, due to different coefficients of thermal expansion in each component. In comparison, the present work addresses the isothermal response of initially stress-free metal matrix composites loaded by an axisymmetric (S-T) stress state, as shown in Fig. 1. The fibers

0956-716X/93 $6.00 + .00

are assumed to be parallel, infinitely long compared to their spacing, and perfectly bonded to the surrounding metal matrix.

Although the cell shown in Fig. 1 is not space filling, periodic conditions are applied to the outer wall at $r = r_m$. The axisymmetric geometry, *S-T* loading, and infinite fiber length greatly simplify the analysis so that the three direct components of stress and strain in the cylindrical coordinate system shown correspond to the principal stress and strain states, (σ_r, σ_θ, σ_z) and (ε_r, ε_θ, ε_z). The corresponding equilibrium equation can be written as (*e.g.*, see [17], pp. 316-323),

$$\frac{\partial \sigma_r}{\partial r} = \frac{\sigma_\theta - \sigma_r}{r}, \qquad (1)$$

and the corresponding compatibility equations consistent with the displacement field $u_r = u_r(r)$, $u_\theta = 0$, $u_z = cz$ are

$$\frac{\partial \varepsilon_\theta}{\partial r} = \frac{\varepsilon_r - \varepsilon_\theta}{r}, \text{ and } \frac{\partial \varepsilon_z}{\partial r} = 0. \qquad (2)$$

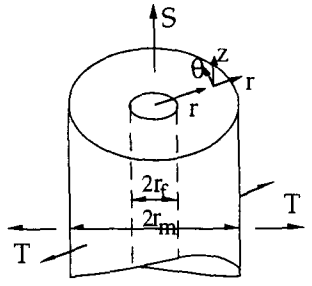

Fig. 1. Axisymmetric cell used to simulate continuous fiber composites.

These equations must be solved subject to boundary conditions that the stresses on the cell boundary match the applied stresses, (*S*, *T*), and that the fiber-matrix interface at $r = r_f$ is fully bonded,

$$\begin{aligned} &\sigma_r(r = r_m) = T, \qquad \varepsilon_\theta^m\big|_{r=r_f} = \varepsilon_\theta^f\big|_{r=r_f}, \qquad \sigma_r^m\big|_{r=r_f} = \sigma_r^f\big|_{r=r_f}, \\ &\frac{1}{\pi r_m^2}\int_0^{r_m} \sigma_z(r) 2\pi r\, dr = S, \qquad \varepsilon_z^m\big|_{r=r_f} = \varepsilon_z^f\big|_{r=r_f}. \end{aligned} \qquad (3)$$

The matrix region, $r_f < r < r_m$, is assumed to be elastic-plastic, and the inner fiber region, $r < r_f$, is assumed to be elastic only. The matrix is assumed to yield when a von Mises yield function defined by

$$\Phi(\sigma_i, \bar{\sigma}_m) = \tfrac{1}{2}[(\sigma_r - \sigma_\theta)^2 + (\sigma_\theta - \sigma_z)^2 + (\sigma_r - \sigma_z)^2] - \bar{\sigma}_m^2 \qquad (4)$$

reaches zero. Here, $\bar{\sigma}_m$ is the current flow stress of the matrix in simple tension, and for isothermal conditions, it is assumed to depend on effective plastic strain, $\bar{\varepsilon}_m^p$. When the yield surface is used as a plastic potential, and conditions of normality and consistency are imposed (*e.g.*, see [17], pp. 77-84), the resulting incremental constitutive relation is

$$d\varepsilon_i^m = \begin{cases} \dfrac{1}{E_m}[(1+\nu_m) d\sigma_i^m - \nu_m d\sigma_{kk}^m], & \Phi < 0 \\ \dfrac{1}{E_m}[(1+\nu_m) d\sigma_i^m - \nu_m d\sigma_{kk}^m] + \dfrac{1}{H}\dfrac{1}{2\bar{\sigma}_m}\dfrac{\partial \Phi}{\partial \sigma_i^m}\left(\dfrac{1}{2\bar{\sigma}_m}\dfrac{\partial \Phi}{\partial \sigma_j^m} d\sigma_j^m\right), & \Phi = 0 \end{cases} \qquad (5)$$

The strain increment in (5) has an elastic contribution dependent on Young's modulus E_m and Poisson's ratio ν_m of the matrix. Here, σ_{kk} denotes the trace of the stress tensor. During yielding, the strain increment has an additional contribution dependent on the plastic modulus, *H*, defined by $d\bar{\sigma}_m / d\bar{\varepsilon}_m^p$. A power-law relation and corresponding plastic modulus of the form,

$$\frac{\bar{\sigma}_m}{\sigma_o} = \left(\frac{\bar{\varepsilon}_m^p}{\varepsilon_o} + 1\right)^N, \quad H = E_m N \left(\frac{\bar{\sigma}_m}{\sigma_o}\right)^{\frac{N-1}{N}} \qquad (6)$$

are used, where σ_o, ε_o are the uniaxial yield stress and strain of the matrix.

The fiber is assumed to be elastic, with different isotropic elastic properties, E_f and ν_f, than the matrix. Under such conditions, the only admissible stress field in the fiber is a uniform one, described by $(\sigma_r^f = \sigma_\theta^f, \sigma_z^f)$ (*e.g.*, see [13], pp. 107-110). Given an increment, $(d\sigma_r^f = d\sigma_\theta^f, d\sigma_z^f)$ in the fiber stress state, the corresponding increment in remote stresses (*S*, *T*) are determined by first using the elastic constitutive relations to find $d\varepsilon_i^f$, then using the continuity conditions in (3) to find $d\varepsilon_\theta^m, d\varepsilon_z^m, d\sigma_r^m$ at $r = r_f$, and finally integrating (1), (2), and

(5) from $r = r_f$ to $r = r_m$. The resulting values of dS, dT are determined using the two relations on the left side of (3). The ratio of $d\sigma_r^f = d\sigma_\theta^f$ to $d\sigma_z^f$ is chosen so that a proportional S-T path is followed from an initially stress-free state to the point where the entire matrix yields. The resulting values of (S,T) for various proportional paths are recorded to produce the entire S-T yield surface.

Results and Discussion

This section describes the anisotropic yield behavior of fiber composites in terms of a departure of the yield surface from a von Mises surface. The principal composite variables considered are the volume fraction, f, of the fiber and the ratio, E_f/E_m, of Young's moduli. Poisson's ratio for each component is usually set to 0.3 in the results shown, although in some specific cases, the values for each component are varied from 0.25 to 0.35. In all cases, the hardening exponent $N = 0.05$ to model an essentially perfectly plastic material with yield stress σ_o, and $\sigma_o/E_m = 0.0004$.

The important yield surface features for the case of stiffer fibers is shown in Fig. 2, where $E_f/E_m = 10$. The dashed line shows the corresponding von Mises surface for the matrix, or equivalently, the surface for $f = 0$, and the solid lines show a succession of approximately elliptical surfaces as f is increased. Over the large range of f shown, the surface becomes more equiaxed and rotates counterclockwise with increasing f. The more equiaxed shape and rotation indicate that both hydrostatic and deviatoric loadings cause yield of these composites. For example, the $f = 0.5$ curve shows that the yield stress in hydrostatic tension is lower than that for pure axial (S) loading. This feature is qualitatively consistent with Chu and Hashin [12], which reports that the hydrostatic stress required to yield a rigid particulate composite with $f = 0.1$ is approximately five times that for $f = 0.5$.

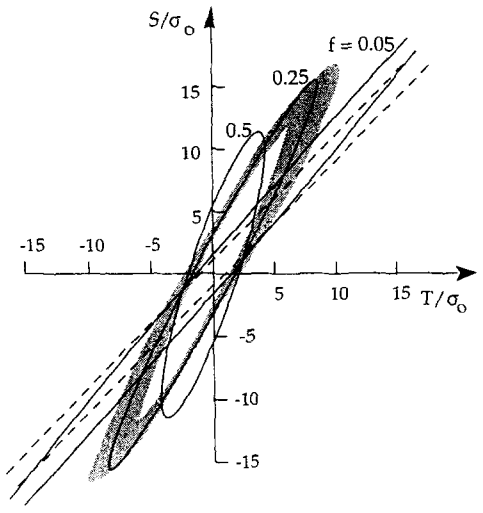

Fig. 2. S-T yield surfaces for composites with E_f/E_m = 10 and $\nu_f = \nu_m = 0.3$ for $f = 0$ (dashed line), 0.05, 0.25, and 0.5 (solid lines). σ_o is the yield stress of the matrix. The shaded region shows the variation in the case for $f = 0.25$ which occurs when ν_f and ν_m are independently varied from 0.25 to 0.35.

The observed rotation in Fig. 2 also introduces anisotropic yield behavior. In particular, the counterclockwise rotation causes the axial yield stress to become larger than transverse one. The rotation also defines a major axis direction, $S \neq T$, along which the composite is most resistant to yield, and a perpendicular minor axis direction, $S \neq -T$, along which the composite is easiest to yield.

Changes in Poisson's ratio of each component generally produces modest variation along the minor axis dimension and much larger variation along the major axis dimension. In particular, the shaded region in Fig. 2 shows the region within which yield surfaces for $f = 0.25$ lie when ν_f and ν_m are varied independently from 0.25 to 0.35. Over this range, the length of the major axis increases in length by approximately 18 percent for the case $\nu_f = 0.25$ and $\nu_m = 0.35$, and decreases by approximately 27 percent when Poisson's ratios are reversed. In comparison, the change in the length of the minor axis is modest. These trends are consistent with Ashby [3], which asserts that yield under hydrostatic loading depends on differences, $\Delta(1/K)$, in bulk moduli of

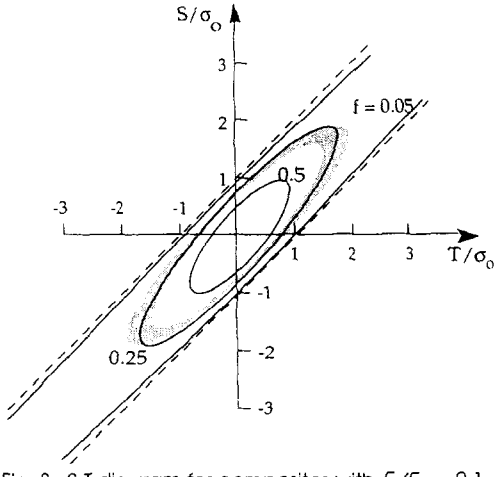

Fig. 3. S-T diagram for composites with $E_f/E_m = 0.1$ and $\nu_f = \nu_m = 0.3$ for $f = 0$ (dashed line), 0.05, 0.25, and 0.5 (solid lines). σ_o is the yield stress of the matrix. The shaded region shows the variation in the case for $f = 0.25$ which occurs when ν_f and ν_m are independently varied from 0.25 to 0.35.

the components. Clearly, in the limit of equal bulk moduli, an admissible solution for hydrostatic loading is that the stress state in each component is simply a uniform hydrostatic stress equal to the applied value. In this limit, the matrix will not yield, and the corresponding yield surface extends indefinitely along the hydrostatic axis. Over the limited range of Poisson's ratios shown for $f = 0.25$, the major axis increases in length and rotates clockwise as the bulk moduli become more similar. In this case, K_f/K_m decreases from approximately 17 for (ν_f, ν_m) = (0.35, 0.25) to 6 when ν_f, ν_m are reversed. Although the case $f = 0.25$ is discussed in detail here, the trend over the range of (ν_f, ν_m) reported is similar for other volume fractions.

The important yield surface features for the case of more compliant fibers are shown in Fig. 3, where $E_f/E_m = 0.1$ and again, Poisson's ratio for each component is 0.3. The trend in rotation is similar to, although less pronounced than that in the stiffer fiber case. Consequently, anisotropy is less pronounced, in that the axial yield stress for a given f is only modestly higher than the transverse value. The reduction in major axis length with f is much larger here, and the minor axis dimension decreases rather than increases, so that all yield surfaces lie within the von Mises ($f = 0$) surface. As for the stiffer fiber case, the shaded region in Fig. 3 shows the locus of yield surfaces for $f = 0.25$ when ν_f and ν_m are independently varied from 0.25 to 0.35. Again, the major axis increases and rotates clockwise as the bulk moduli of each component become more equal. Results for a hollow spherical shell of rigid perfectly plastic material show a similar reduction in major and minor axes, but no rotation occurs in that case [14].

Figures 4, 5 and 6 document, respectively, the yield surface orientation θ, length a of the major axis, and length b of the minor axis over a wide range of fiber volume fraction and ratio of Young's moduli of the two components, with $\nu_f = \nu_m = 0.3$. These three quantities may be used to define elliptical yield surfaces that reasonably approximate the computed ones. Using this approximation, the yield values for pure axial loading (S_y), pure axisymmetric loading (T_y), and hydrostatic loading (P_y) are simply functions of a, b, and θ provided by these plots,

$$S_y = \pm\left(\frac{a^2b^2}{a^2\cos^2\theta + b^2\sin^2\theta}\right)^{1/2} \approx \pm\frac{b}{\cos\theta} \text{ for } f << 1 \tag{7}$$

$$T_y = \pm\left(\frac{a^2b^2}{a^2\sin^2\theta + b^2\cos^2\theta}\right)^{1/2} \approx \pm\frac{b}{\sin\theta} \text{ for } f << 1 \tag{8}$$

$$P_y = \pm\left(\frac{2a^2b^2}{(a^2+b^2)+(b^2-a^2)\sin 2\theta}\right)^{1/2} . \tag{9}$$

The orientation angle θ is a basic measure of anisotropy, in that the ratio, $S_y/T_y = \tan\theta$ in the dilute (small f) limit, where $a >> b$. Further, the loading paths $S/T = \tan\theta$, $\tan\theta \pm 90°$ are the directions along which the composite is most resistant and least resistant to yield, respectively.

The plot of yield surface orientation in Fig. 4 shows that $\theta = 45°$ when the elastic properties of the fiber and matrix are equal, and that θ increases when the fiber and matrix moduli become more different, regardless of whether the fibers are more or less stiff. In fact, θ for the case of cylindrical voids, approximated by $E_f/E_m = 10^{-4}$, is comparable to that for stiff fibers in the range $E_f/E_m \approx 5$ to 8. In all cases, the rotation appears to increase most rapidly with f in the dilute range.

Figure 5 demonstrates that the major axis of the yield surface decreases in length as the fiber and matrix moduli become more different. Clearly, the effect is much more pronounced for less stiff fibers. In the limiting case of cylindrical voids, modeled by $E_f/E_m = 10^{-4}$, the length a of the major axis is comparable to the external hydrostatic stress, $P_y = -2\ln(f)/3$ to yield a thick-walled spherical shell surrounding a spherical void of volume fraction f [13]. In comparison, the minor axis of the yield surface increases or decreases in length as the fiber is made more stiff or more compliant, respectively, than the matrix. In the more dilute limit, the major axis length a is a measure of the composite resistance to hydrostatic loading, while the minor axis limit b is a measure of the composite resistance to deviatoric and uniaxial loading. The comparison in Figs. 4, 5, 6 with results from finite element based results [5] suggests that the non space-filling cell employed here reasonably approximates θ and b for arrays of hexagonally packed fibers with $E_f/E_m = 6$ and (ν_f, ν_m) = (0.21, 0.33), although it appears to overestimate a. However, the finite element work [5] is based on onset of yield in the matrix compared to full matrix yield in the present work. In general, packing geometry has little effect on axial yield, although it does have strong effects on transverse yield behavior [9, 10].

The anisotropy present in a cylindrical geometry is apparent when model predictions for $E_f/E_m \to 0$ are compared with an isotropic yield function proposed by Gurson for a plastic spherical shell with void volume fraction f [15]. Gurson's yield function can be written as

$$\Phi = \frac{3}{2}\frac{\sigma'_{ij}}{\bar{\sigma}_m}\frac{\sigma'_{ij}}{\bar{\sigma}_m} + 2f\cosh\left(\frac{3\sigma_{kk}}{2\bar{\sigma}_m}\right) - (1+f^2) = 0 , \tag{11}$$

where $\sigma'_{ij} = \sigma_{ij} - \sigma_{kk}/3$ is the stress deviator and $\bar{\sigma}_m$ is the flow stress of the matrix. Figure. 7 shows a comparison between the two models for $f = 0.2$. The most apparent change when the void shape is changed from spherical to cylindrical is that both the major and minor axes of the yield surface decrease, and the yield surface rotates counterclockwise. The decrease in the size of the yield surface and rotation associated with a spherical to cylindrical change in void shape contribute to a lower yield under both hydrostatic (P) and transverse (T) loadings, but provide a comparable yield for axial (S) loading.

Figure 7 also shows that the cylindrical shell model, although not space filling, provides a reasonable approximation to more realistic finite element analyses of spheroidal voids periodically embedded in a perfectly plastic matrix [16]. Figure 7 shows that the yield surface produced for a cubic array of spheroids with $f = 0.2$, which are nearly connected along the S dimension (the aspect ratio of S to T dimensions is 2.5 to 1), is very similar in size, shape, and orientation to the cylindrical shell model employed in this paper.

Conclusions

An axisymmetric cylindrical cell containing a cylindrical elastic fiber in the center, surrounded by an annulus of elastic perfectly plastic matrix, was used to determine the yield properties of continuous fiber composites subject to axisymmetric (S-T) loading. Although the matrix is assumed to obey a pressure-independent von Mises yield criterion, composites with different bulk moduli for each component yield under

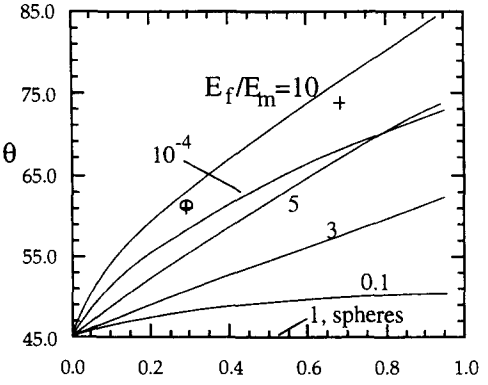

Fig. 4. Orientation angle θ of the major axis of S-T yield surfaces as a function of fiber volume fraction and ratio of Young's moduli, for $\nu_f = \nu_m = 0.3$. (+) denotes finite element based estimates from (5), and (o) denotes self-consistent based estimates from (11); both assume $E_f/E_m = 6$, $\nu_f = 0.21$, $\nu_m = 0.33$.

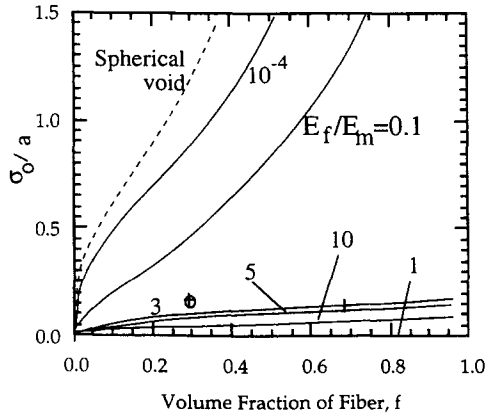

Fig. 5. The length of the major axis of S-T yield surfaces, as a function of fiber volume fraction and ratio of Young's moduli, for $\nu_f = \nu_m = 0.3$. The dashed line shows the prediction for spherical voids based on (13). See Fig. 4 caption for meaning of (+), (o).

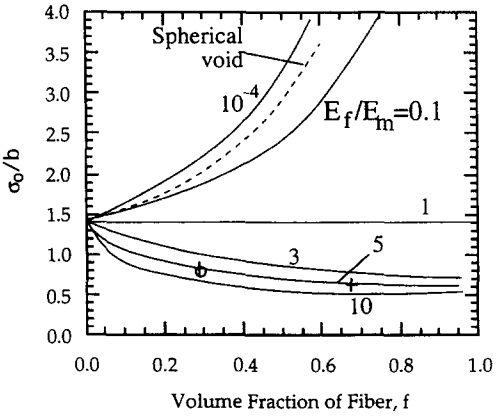

Fig. 6. The length of the minor axis of S-T yield surfaces, as a function of fiber volume fraction f and ratio of Young's moduli, for $\nu_f = \nu_m = 0.3$. The spherical void result is based on (15). See Fig. 4 caption for meaning of (+), (o).

pure hydrostatic loading. The analysis shows that the hydrostatic load to yield decreases with increasing difference in bulk modulus of the components, regardless of which component has the higher bulk modulus.

Continuous fiber composites are also shown to have preferred axisymmetric loadings for which they are most resistant and least resistant to yield. Although the matrix material is most resistant to yield when $|S| = |T|$, the composites tend to be most resistant to yield for specific loadings with the general feature $|S| > |T|$, regardless of whether the fiber is more or less stiff than the matrix. In a related manner, each composite has (S-T) loading directions for which it is easiest to yield, which differ from the von Mises prediction that $|S| = -|T|$. These features are linked to an inherent anisotropy in fiber composites, the magnitude of which is quantified in terms of a rotation of the (S-T) yield surface that is dependent on the relative elastic properties and volume fraction of the fiber. The large rotations observed over a wide range of elastic properties and volume fractions suggest important design criteria that are not modeled well by isotropic theories of yielding.

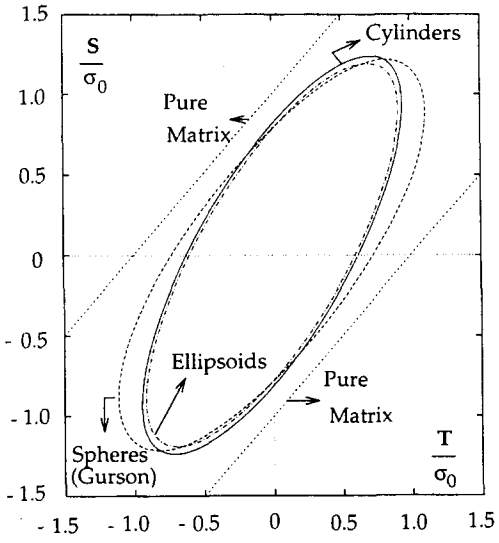

Fig. 7. Comparison of the S-T predictions for porous materials with $f = 0.2$, assuming a continuous cylindrical void shape, nearly connected ellipsoids (16), and spherical voids (15). The pure matrix curve is a von Mises surface.

Acknowledgments

Financial support for HZ and GSD were provided by the Army Research Office under grant 30608-MSYIP, W. Simmons, Contract Monitor; SK was supported by Engineering Research Center, Ohio State University under contract 722123; PMA was supported by the Office of Naval Research contract N00014-91-J-1998 with R. Barsoum, contract monitor. The authors are also thankful for support by the Ohio Supercomputer Center at Ohio State University under Grants PAS-676-1 and 647-3.

References

1. R. Hill, *J. Mech. Phys. Solids* **12**, 213 (1964).
2. J.F. Mulhern, T.G. Rogers, and A.J.M. Spencer, *J. Inst. Maths Applics* **3**, 21 (1967).
3. M.F. Ashby, S.H. Gelles, and L.E. Tanner, *Phil. Mag.* **18**, 757 (1969).
4. S. V. Radcliffe, *Irreversible Effects of High Pressure and Temperature on Materials*, ASTM STP 374, pp. 141-62 (1964).
5. G.J. Dvorak, M.S.M. Rao, and J.Q. Tarn, *J. Comp. Mater* **7**, 194 (1973).
6. G.J. Dvorak, M.S.M. Rao, and J.Q. Tarn, *J. Appl. Mech.* **41**, 249 (1974).
7. G.S. Daehn, P.M. Anderson, and H. Zhang, *Scripta Metall. Mater.*, **25**, 2279 (1991).
8. H. Zhang, P. M. Anderson, and G. S. Daehn, submitted to *Metall. Trans.*, April, 1993.
9. J.R. Brockenborough, S. Suresh, and H.A. Wienecke, *Acta metall. mater.* **39**(5), 735 (1991).
10. T. Nakamura and S. Suresh, *Acta metall. mater.* **41**(6), 1665 (1993).
11. G.J. Dvorak and Y.A. Bahaei-El-Din, *J. Mech. Phys. Solids* **27**, 51 (1979).
12 T.Y. Chu and Z. Hashin, *Int. J. Engrg. Sci.* **9**, 971 (1971).
13. Hill, R., *The Mathematical Theory of Plasticity*, Oxford University Press, 1950.
14. M. Oyane, M. Omura, T. Tabata, and T. Hisatsune, *Ingenieur-Archiv* **59**, 267 (1989).
15. A.L. Gurson, *ASME J. Engng. Materials Tech.*, **99**, 2-15 (1977).
16. S. Krishnaswami, and P. M. Anderson, unpublished work, August, 1993.
17. J. Chakrabarty, *Theory of Plasticity*, McGraw-Hill, 1987.